Focused methane migration formed pipe structures in permeable sandstones: Insights from uncrewed aerial vehicle-based digital outcrop analysis in Varna, Bulgaria

CHRISTOPH BÖTTNER[*,1] (iD), BEN J. CALLOW† (iD), BETTINA SCHRAMM* (iD), FELIX GROSS‡ (iD), JACOB GEERSEN* (iD), MARK SCHMIDT* (iD), ATANAS VASILEV§ (iD), PETAR PETSINSKI§ and CHRISTIAN BERNDT* (iD)

*GEOMAR Helmholtz-Centre for Ocean Research Kiel, Wischhofstraße 1-3, Kiel, 24148, Germany (E-mail: christoph.boettner@ifg.uni-kiel.de)
†Ocean and Earth Science, University of Southampton, University Road, Southampton, SO17 1BJ, UK
‡Center for Ocean and Society, University of Kiel, Kiel, Germany
§Institute of Oceanology – Bulgarian Academy of Sciences, 40 Parvi may str., PO Box 152, Varna, 9000, Bulgaria

Associate Editor – Kevin Taylor

ABSTRACT

Focused fluid flow shapes the evolution of marine sedimentary basins by transferring fluids and pressure across geological formations. Vertical fluid conduits may form where localized overpressure breaches a cap rock (permeability barrier) and thereby transports overpressured fluids towards shallower reservoirs or the surface. Field outcrops of an Eocene fluid flow system at Pobiti Kamani and Beloslav Quarry (*ca* 15 km west of Varna, Bulgaria) reveal large carbonate-cemented conduits, which formed in highly permeable, unconsolidated, marine sands of the northern Tethys Margin. An uncrewed aerial vehicle with an RGB sensor camera produces ortho-rectified image mosaics, digital elevation models and point clouds of the two kilometre-scale outcrop areas. Based on these data, geological field observations and petrological analysis of rock/core samples, fractures and vertical fluid conduits were mapped and analyzed with centimetre accuracy. The results show that both outcrops comprise several hundred carbonate-cemented fluid conduits (pipes), oriented perpendicular to bedding, and at least seven bedding-parallel calcite cemented interbeds which differ from the hosting sand formation only by their increased amount of cementation. The observations show that carbonate precipitation likely initiated around areas of focused fluid flow, where methane entered the formation from the underlying fractured subsurface. These first carbonates formed the outer walls of the pipes and continued to grow inward, leading to self-sustaining and self-reinforcing focused fluid flow. The results, supported by literature-based carbon and oxygen isotope analyses of the carbonates, indicate that ambient seawater and advected fresh/brackish water were involved in the carbonate precipitation by microbial methane oxidation. Similar structures may also form in modern settings where focused fluid flow advects fluids into overlying sand-dominated formations, which has wide implications for the understanding of how focusing of fluids works in sedimentary basins with broad consequences for the migration of water, oil and gas.

[1]Present address: Institute of Geosciences, Christian-Albrechts-Universität zu Kiel, Kiel, Germany

INTRODUCTION

Fluids play an important role in the evolution of marine sedimentary basins. Fluid abundance and composition are primarily governed by flow along permeable beds or focused flow across geological formations (Whitaker, 1986; Berndt, 2005). Seismic data have revealed focused fluid flow conduits in various geological settings around the world, manifesting themselves in a wide range of seismic anomalies (Cartwright, 2007; Løseth *et al.*, 2009; Andresen, 2012; Karstens & Berndt, 2015). Seismic imaging is an effective way to investigate fluid flow systems because acoustic impedance and seismic wave attenuation are highly sensitive to pore space filling (White, 1975). This sensitivity allows the imaging and interpretation of basin-scale fluid flow systems, subsurface geometries, fluid accumulations and permeability barriers (Berndt, 2005; Cartwright, 2007). However, there is an observational gap between seismic data (several metre-scale) and geological field mapping (millimetre-scale to centimetre-scale) of natural fluid flow systems.

Field observations and geological sampling from exhumed ancient fluid flow systems can constrain their internal architecture, the diagenetic interaction of fluids with the bedrock and physical properties of flow processes (De Boever *et al.*, 2006a; Huuse *et al.*, 2010; Capozzi *et al.*, 2015; Nelson *et al.*, 2017). The comparison of field observations from ancient fluid flow systems with seismic data from modern marine sedimentary systems can narrow the interpretation gap between seismic and sub-seismic scales, for example, below 4 m vertical resolution of high-resolution three-dimensional P-cable seismic data (Planke & Berndt, 2007).

Uncrewed aerial vehicles (UAVs) equipped with high-resolution optical RGB sensor cameras represent a cost-effective and efficient way to map complex geological patterns in 3D providing kilometre-scale maps of fluid flow features in terrestrial outcrops with centimetre-resolution (e.g. Bemis *et al.*, 2014). This yields valuable information on the spatial distribution patterns and internal architecture. Combination with field observations and rock sampling provides a further insight into the interaction between fluid flow and the bedrock and hydraulic properties, especially permeability (Bisdom *et al.*, 2017).

Pobiti Kamani, located 20 km north-west of Varna, Bulgaria, hosts several hundred ancient carbonate-cemented tubular concretions (hereafter referred to as 'pipes') which are up to 10 m high (De Boever *et al.*, 2006a,b). The cemented pipes are the largest exposed hydrocarbon-derived carbonate conduits known globally and are well-exposed in the unconsolidated sands and lithified sandstones of the Dikilitash Formation (Sinclair *et al.*, 1998; De Boever *et al.*, 2006a; Capozzi *et al.*, 2015). At Beloslav Quarry, an old sand extraction quarry near the Village of Beloslav, the pipes crop out along a *ca* 40 m high cliff which provides the opportunity to map their spatial distribution and vertical extent (De Boever *et al.*, 2009a).

Focused fluid flow in marine settings, which is primarily dependent on the hydraulic parameters of the hosting sediments, is predominantly observed through faults and fracture networks in low permeability silty to muddy sediments or lithified rocks (e.g. Judd & Hovland, 2007; Böttner *et al.*, 2019). It is far less clear how fluids can stay focused in permeable sand because the high permeability should allow fluids to disperse. Nevertheless, the hydrocarbon-derived carbonate conduits unequivocally document focused fluid flow in the unconsolidated sand of the Dikilitash Formation in the study area (De Boever *et al.*, 2006a,b). Similar but much smaller pipe structures also exist in the Kattegat, Denmark or on the Montenegrin margin, Adriatic Sea (Jørgensen, 1992; Angeletti *et al.*, 2015).

The aim of this study is to analyze the pipe-forming processes within sand formations using the two outcrops at Beloslav Quarry and Pobiti Kamani. The objectives are to first evaluate the structural control on seep location and determine the influence of regional and local tectonic deformation on pipe location. Second, the involved fluids and key pre-conditions for focused fluid flow and subsequent formation of pipes in sand formations are identified and characterized. This includes constraining the temporal evolution of such pipe formation during the Eocene; and, third, the geological setting in which such pipes may form is assessed.

GEOLOGICAL SETTING

The Pobiti Kamani natural park covers an area of about 253 ha within the Varna depression, along the eastern side of the Alpine Balkanides. It forms a section of the Moesian Platform, a tectonic unit that extends from northern Bulgaria to southern Romania (Bergerat *et al.,* 1998; Georgiev *et al.,* 2001). The Moesian Platform was likely part of a block-faulted Triassic to Oligocene siliciclastic shelf and carbonate succession along the northern Tethys margin (Sinclair *et al.,* 1998). Several hundreds of calcite-cemented tubular concretions (hereafter referred to as pipes; Fig. 1; Botz *et al.,* 1993; De Boever *et al.,* 2006a,b, 2009a,b, 2011a,b) are hosted in the Dikilitash Formation. This formation comprises alternating sequences of unconsolidated silt to sand sediments with interbeds of calcite-cemented sandstones (Fig. 1). The Dikilitash Formation is *ca* 40 m thick and was deposited in the Early Eocene in a mid to outer ramp depositional system at water depths around 100 m (De Boever *et al.,* 2006a, 2009a,b).

The pipes are 0.5 to 3.0 m in diameter and up to 10 m high. Groups of pipes have been documented at several locations dispersed over an area of 70 km², including the Central, Strashimirovo, Beloslav Quarry, Banovo and Teterlik groups (Fig. 1; De Boever *et al.,* 2009a,b, 2011a,b). These groups align along Palaeogene NNE–SSW trending transtensional faults that have up to 80 m vertical displacement (Bergerat *et al.,* 1998; De Boever *et al.,* 2009b). The co-location of the groups with the Palaeogene faults suggests a structural control on the location of the pipes (De Boever *et al.,* 2009b).

Geochemical analyses of the calcite-cemented tubular concretions show that they formed from ascending methane-rich fluids resulting in low-Mg carbonate precipitation (Botz *et al.,* 1993; De Boever *et al.,* 2006a,b, 2009a,b). Stable carbon isotope composition of carbonates of about −43 to −45‰ Vienna Pee Dee Belemnite (V-PDB; Botz *et al.,* 1993; De Boever *et al.,* 2006a) and heavily depleted $\delta^{13}C$ isotope ratios of archaeal biomarker ($\delta^{13}C$ −123 to −81‰ V-PDB; De Boever *et al.,* 2009a) indicate that the exposed pipes and calcite cemented interbeds likely formed because of microbially mediated anaerobic oxidization of methane at or below the seafloor. The corresponding fluids likely migrated along the transtensional faults into the Dikilitash Formation (De Boever *et al.,* 2009b). Based on oxygen isotope ratios of carbonates the environmental conditions during formation were correlated with Lower Eocene marine environment (age *ca* 50 Ma; De Boever *et al.,* 2006a). There are two distinct groups of pipes with differing $\delta^{13}C$ and $\delta^{18}O$ isotope ratios. Group 1 carbonates ($\delta^{13}C$ *ca* −45 to −35‰ V-PDB and $\delta^{18}O$ ±1‰ V-PDB) likely formed because of fluids from below that included biogenic methane and ancient sea (salt) water. Group 2 carbonates ($\delta^{13}C$ <−25‰ V-PDB and $\delta^{18}O$ <−6.5‰ V-PDB) are characterized by alteration of the isotope ratios likely due to mixing of ascending methane with marine dissolved inorganic carbon (DIC) ($\delta^{13}C$ *ca* 0‰) and/or δ^{13}-enriched CO_2 and recrystallization because of percolating Cenozoic meteoric water (De Boever *et al.,* 2009a). These distinct groups appear in alternating concentric bands from the centre of the carbonate conduits (De Boever *et al.,* 2006a).

METHODS

An uncrewed aerial vehicle (UAV, DJI Inspire 2), equipped with a 20.8 MP Zenmuse X5S (RGB channels) camera and a DJI MFT 15 mm/1.7 ASPH lens (SZ DJI Technology Company Limited, Shenzhen, China), was used to acquire images of the Pobiti Kamani area and Beloslav Quarry (Fig. 2). The images were stored in .jpg format. The flight surveys were designed with DJI GroundStationPro, and the surveys were subsequently flown automatically by the UAV. This procedure results in a very regular flight pattern and good overlap of neighbouring images (overlap: front 90%, sides 60%; shot interval: 2 s; speed: 2.6 m s^{-1}). For the Beloslav Quarry, manually controlled surveys were conducted to achieve better coverage of the cliff, which represents the 80 m high surface expression of a transtensional fault. The average flight time was *ca* 25 min with rolling shutter set to 2 to 3 s resulting in a data set of more than 4500 images (*ca* 42 GB) for the 200 by 600 m wide Pobiti Kamani area and more than 2000 images (*ca* 25 GB) for the 400 by 1200 m wide area of Beloslav Quarry.

The commercial software Pix4D$^{™}$ was used to calculate the digital elevation model (DEM), a point cloud, and an ortho-rectified mosaic (RGB) by the structure from motion (SfM) approach. For the Pobiti Kamani area, the resolution of the derived ortho-rectified mosaic, point cloud and DEM resolution is *ca* 1 cm per pixel. Ten ground control points were used to adjust the geo-referencing of the results. Real-time kinematic (RTK) service was not available during the acquisition
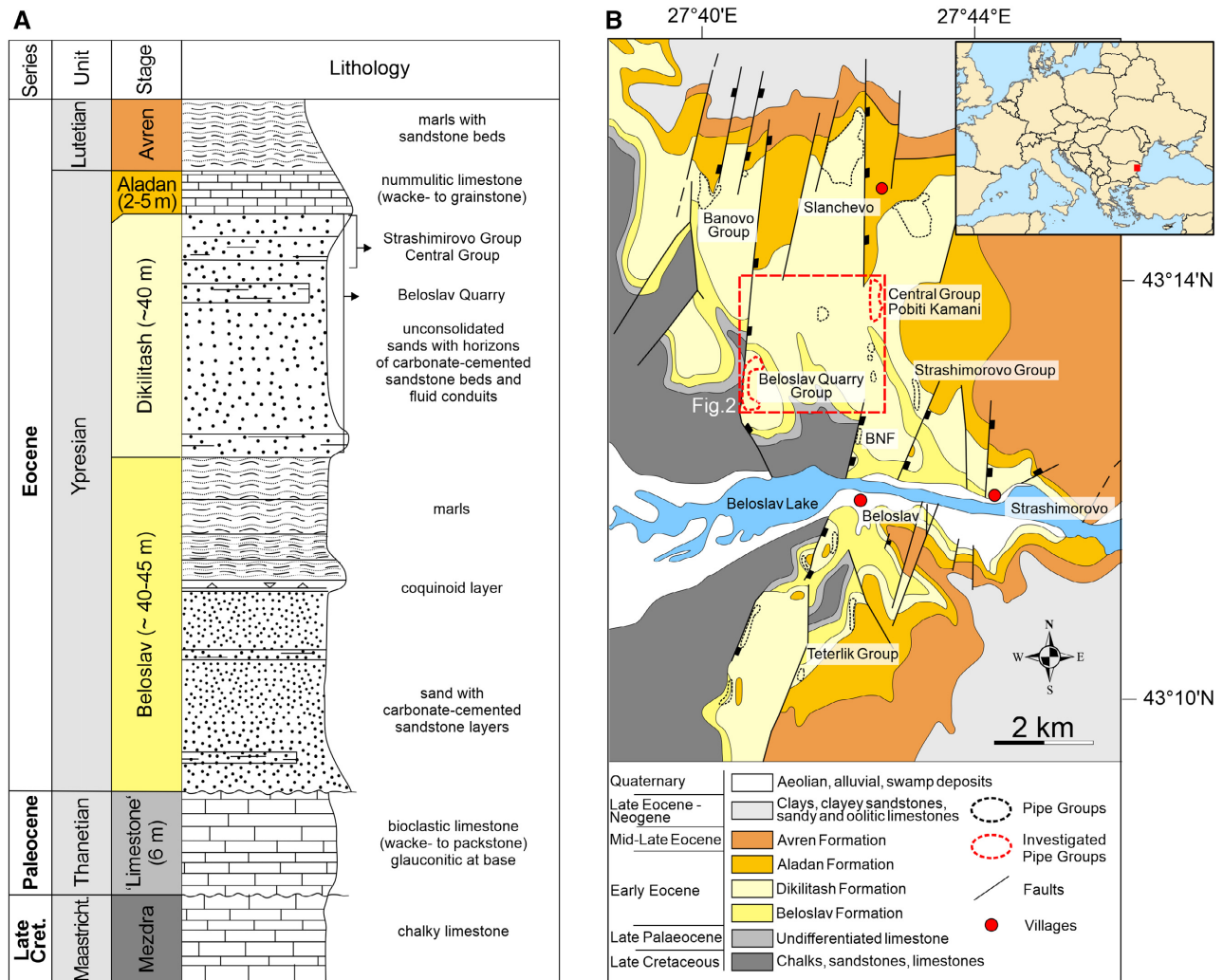
Fig. 1. (A) Stratigraphic column with the main lithologies (with highlighted formations in which the pipes appear) and (B) simplified geological setting of the survey area. Investigated pipe groups are highlighted with red dotted lines. BNF = Beloslav North fault (modified after De Boever *et al.,* 2009b). The small inset shows a red square with the location of the simplified geological map. The red dashed box shows the location of Fig. 2.

campaign, resulting in a minimum accuracy of the location of the overall model of 1.3 ± 0.6 m. The Beloslav Quarry area is hard to access because of the high relief and thus ground control points could not be established, resulting in a location accuracy of *ca* 2 m. The resolution of the Beloslav Quarry model is *ca* 2 cm per pixel.

Surface fractures and pipes were manually picked in the ortho-rectified mosaic to analyze the spatial distribution of the pipe structures and fractures. The manual picking of *in situ* pipes was validated with outcrop observations, ensuring the omission of eroded pipes which are not *in situ*. Multiple ESRI ArcGIS (version 10.6) geoprocessing tools delineate the outlines

of the pipes. In the first step, the inverse of the DEM was calculated, and all depressions filled. Subsequently a differential grid was calculated by subtracting the original DEM from the filled DEM and classified all regions that had changed by more than 0.1 m. After automatically drawing outlines around the classified areas, all generated polygons that did not include one of the manually picked pipe structures were removed. This step was necessary to remove trees and houses, which were also picked and outlined by the workflow. In a final step, all polygons were inspected manually, and some were edited due to their proximity to trees or eroded pipe fragments which resulted in enlarged polygons.
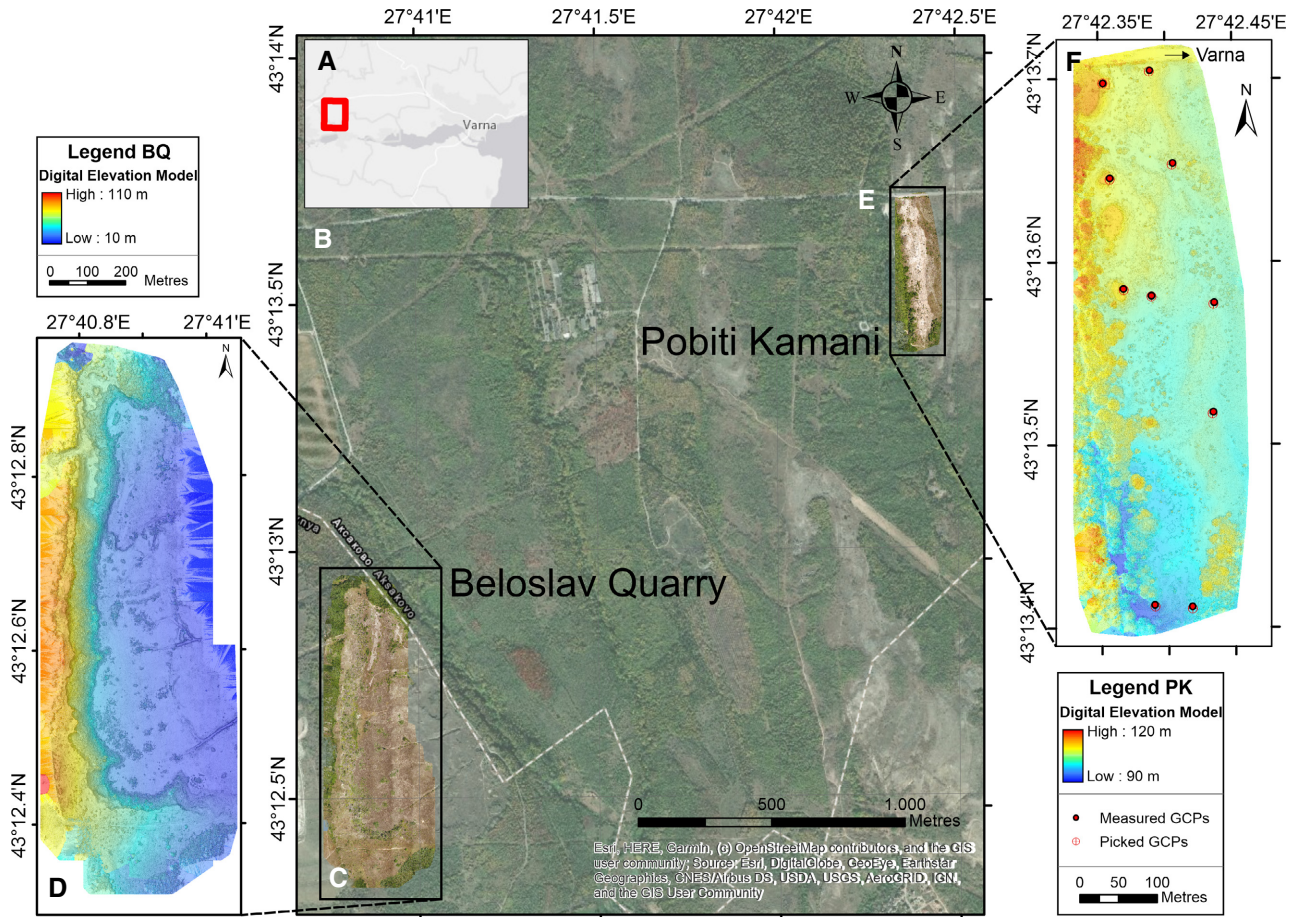
Fig. 2. Overview map of the survey areas located 20 km west of Varna, Bulgaria. (A) Regional map showing the location of the investigated areas in a red box. (B) Local map of the two investigated outcrops of Pobiti Kamani and the Beloslav Quarry (white boxes). Black lines indicate the approximate location of normal faults in the area (modified from De Boever *et al.,* 2006a). (C) Ortho-rectified image mosaic of Beloslav Quarry and (D) corresponding SfM-derived digital elevation model (DEM). (E) Ortho-rectified image mosaic of Pobiti Kamani and (F) corresponding DEM. Red dots indicate measured ground control points (GCPs) and red crosses the picked GCPs.

During the analysis of the spatial distribution of pipes, the pattern analyses tool 'z-score' was used. The z-score is the standard deviation that a given population distribution deviates from a normal distribution. It provides a measure of clustering. A z-score below −2.58 indicates the presence of clustering, with a below 1% likelihood that the clustering is statistically random.

The UAV-based photogrammetric SfM allows rapid mapping of pipes and tectonic deformation structures over large areas (tens of square kilometres). However, ground-based geological mapping and sampling is necessary to analyze the composition, texture and geometry of the pipes, to understand further the relationship between the pipes with the surrounding host sediment and the sub-horizontal interbeds. Field samples were collected with a hand-held drill with a 32 mm diamond drill bit to compare the composition and texture of the pipes with the surrounding host rock and the carbonate beds. Samples were collected along vertical and horizontal transects across single well-exposed pipes to a maximum depth of 25 mm into the carbonates and sample orientation was documented. Thin sections (30 μm thickness) were prepared and mounted onto glass slides, for petrological analysis and scanning electron microscopy (SEM). The samples were impregnated with blue epoxy resin, highlighting the pore space. A total of 18 thin sections were prepared and analyzed using a polarizing microscope. The SEM imaging was conducted with a Carl Zeiss Leo 1450 VP scanning electron microscope (SEM) with an energy
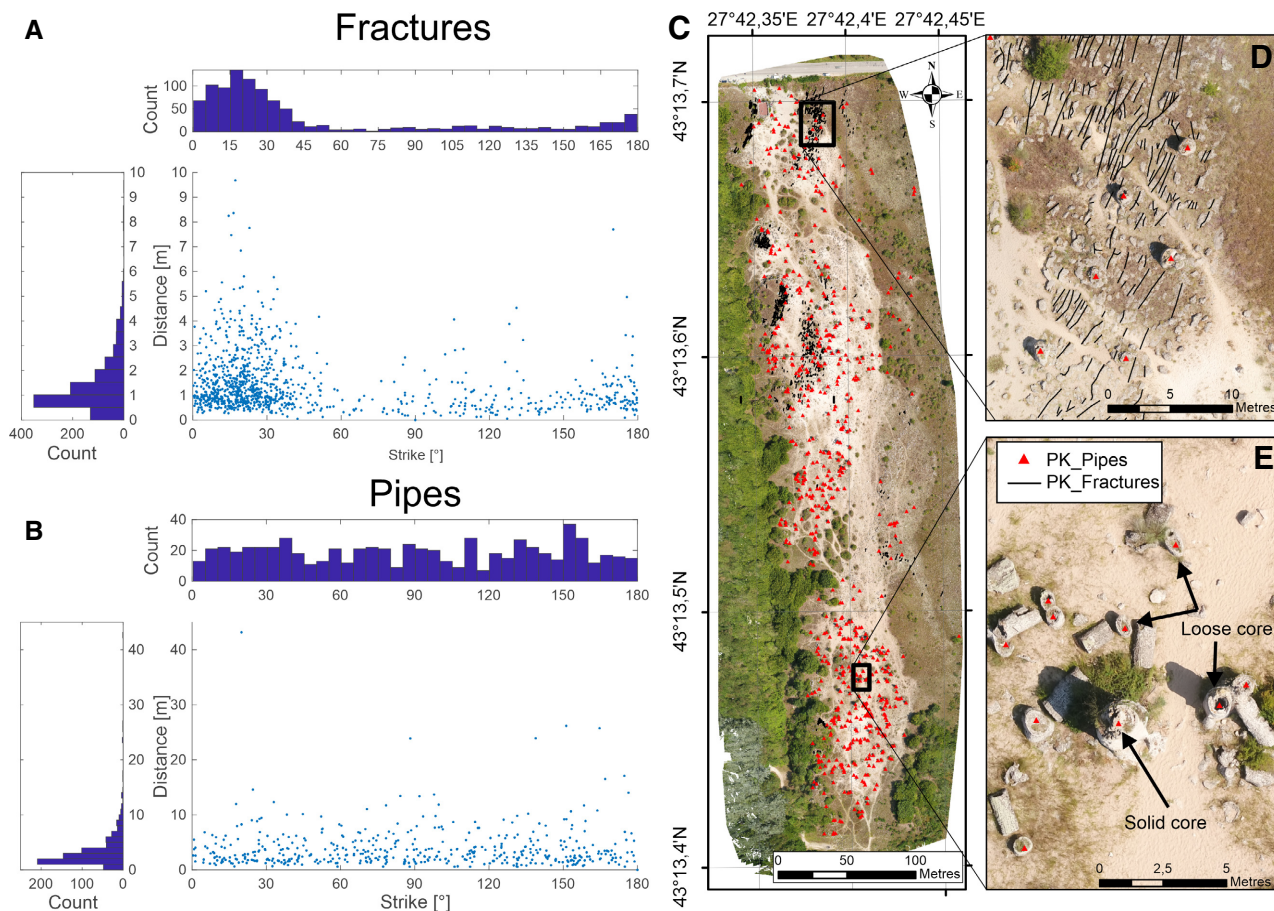
Fig. 3. Uncrewed aerial vehicle (UAV)-based orthomosaic map from Pobiti Kamani. (A) Scatterplot for fractures of their strike direction against measured length and corresponding histograms showing the frequency of both per unit. (B) Scatterplot for pipes and their nearest neighbour direction against nearest neighbour distance and corresponding histograms showing the frequency of both per unit. (C) UAV-based ortho-rectified image of Pobiti Kamani with manually picked pipes and fractures. Black boxes show the location of (D) and (E); red triangles show pipe location and black lines indicate fractures. (D) The pipe location with respect to the fractures and (E) the location of pipe with respect to each other and the appearance of single pipes (loose inner core and solid inner core). PK = Pobiti Kamani.

dispersive spectrometer (EDX) (Carl Zeiss AG, Jena, Germany). The samples were carbon coated and imaged at a spatial resolution of 700 nm. From the SEM image data, the contrast between mineral phases is determined by their relative X-ray attenuations (Ketcham & Carlson, 2001). There was a significant image contrast between each mineral phase, allowing the calculation of each phase, accurate to the nearest percent. The SEM-EDX analysis verified the elemental composition of each phase. Using the method approach described in Callow *et al.* (2020), image processing of the SEM images was done using ImageJ software to obtain calculations of porosity, mineral area fractions, as well as grain and pore size distributions.

RESULTS

Mapping and analyses of spatial distribution

Pobiti Kamani

The data set comprises 672 individual pipes, 42 individual calcite-cemented interbed exposures covering at least 945 m² and 1016 individual fractures with a total length of 1471 m and a mean length of *ca* 1.45 m (Fig. 3). These fractures are predominantly oriented in a NNE–SSW strike direction with a *ca* 90° dip, which is validated with field measurements (Fig. 3A). The pipes in Pobiti Kamani are highly clustered (average nearest neighbour, z-score: −13.33) with

an average distance between nearest pipes of 3.58 ± 3.38 m (maximum 43.16 m; Fig. 3B). The pipe distribution is densely spaced with a maximum of one pipe per 14.3 m^2 (mean: one pipe per 36.7 m^2). There is no predominant pipe cluster strike direction, nor can a direct relationship be discerned between fracture geometries and pipe location (Fig. 3A versus 3B; 3D) as suggested by De Boever *et al.* (2009b).

For Pobiti Kamani, approximately one fifth of pipes show predominantly solidified inner cores (*ca* 22%). The majority of pipes (*ca* 78%) have unlithified inner cores (Fig. 3E). The outlines of the pipes allow for assessing of geometric parameters from the high-resolution DEM. The average, maximum and minimum values are summarized in Table 1. The horizontal eccentricity and area versus perimeter parameters indicate less complex, subrounded circular features.

The data analyses of the pipes are limited by the extent of the surveyed area. There are more pipes to the north and to the south, which are not part of the orthomosaic map. The DEM suggests that the pipes occur in the hangingwall side of the NNE–SSW striking Palaeogene transtensional faults. However, the fault contact that would constrain the pipe location towards the west is not visible in the orthomosaic or DEM maps.

Beloslav Quarry
The 3D point cloud was used in combination with the original RGB-images to manually pick the pipes on different elevation levels. The point cloud shows that the pipes are separated by at least seven distinct interbeds, separating the pipes into tiers (colour coded triangles between I1 to I7; see Fig. 4B). These interbeds show sub-horizontal bedding with a slight dip of less than 10° in a south-eastern direction (Fig. 4B) and consists of calcite-cemented sandstones that separate the beds of unconsolidated silt to sand sediments which host the pipes.

The data set comprises 1066 individual pipes and large carbonate interbed exposures covering more than 1600 m^2, but the coarser resolution of this data set and denser vegetation prohibit digital analyses of fractures. Spatial analyses of the pipes show that they are highly clustered (average nearest neighbour *z*-score: −37.84) and have a neighbouring distance of 2.24 m ± 3.38 m (maximum 55.47 m, minimum 0.04 m). The pipes are densely spaced with an average of one pipe per 13.6 m^2 (maximum one pipe per 4.6 m^2). There is no preferred pipe cluster orientation observed from the data.

Field observations

Field observations within the Beloslav Quarry are used to characterize the geometry of the carbonate pipes and their relation to the surrounding host strata. Carbonate pipes of metre-scale diameter (Fig. 5A) protrude from a light grey sand bed. The lack of bedding in the host sediment intervals is evidence for significant bioturbation or sediment reworking. The carbonate pipes are orientated sub-vertically and perpendicular to the carbonate horizons (Fig. 5B and C). The pipes are metre-scale in width and appear to occur in discrete clusters (Fig. 5D). There is no evidence that the spatial distribution of the individual clusters follows any regular pattern and the distance between individual pipes (*ca* 2 to 4 m) fits the results from the orthomosaic analyses. Many carbonate pipes bifurcate upward (Fig. 4E) confirming interpretations based on the UAV raw imagery. However, the convergence of pipes also occurs in some places (two pipes merging into one; see Fig. 5). More complex geometries where pipes appear intertwined are also observed.

All pipes show a more globular or bulbous outer surface towards their top (Fig. 5F), which often correlates with overlying calcite cemented interbeds. The interbeds dip down slightly towards the pipes, highlighting a direct relationship between the pipes and calcite cemented interbeds (Fig. 5G). There appear to be two main calcite cemented interbeds of metre-scale thickness, comprising an upper (Fig. 5G) and lower interbed (Fig. 5H). Furthermore, the base of the calcite cemented interbeds display a branching network of burrows, similar in morphology to the interpreted vertical burrows on the outer margin of the pipes (Fig. 5L).

The colour of the host sand bed is the same as that of unweathered pipes (Fig. 5I). The outer boundary between the carbonate pipe and the surrounding host rock is sharp in weathered examples, but slightly more diffuse in unweathered examples (Fig. 5I to K). The host sediment is composed of poorly consolidated, quartz sand with minor micritic cement (Figs 5I and 6A). The overall bed is heavily bioturbated, with an abundance of shell fragments and nummulites, ranging from 0.5 to 25 mm in diameter (Fig. 6), providing evidence for an outer ramp depositional environment (Fig. 5M).

To ground truth the orthomosaic map and DEM, fracture distribution, orientation and dip was measured in the field. For Pobiti Kamani,

Table 1. Geometric parameters from high-resolution digital elevation model (DEM) and polygons of pipes within Pobiti Kamani include area, perimeter, maximum height, minimum and maximum width, and derived parameters such as the ratio between area and perimeter, the eccentricity, and volume as well as spatial information on the distance to their nearest neighbour.

Geometric parameter	Area [m²]	Perimeter [m]	Maximum height [m]	Minimum width [m]	Maximum width [m]	Area/ Perimeter [m]	Eccentricity	Volume [m³]	Nearest neighbour [m]
Minimum	0.05	0.76	0.00	0.24	0.24	0.06	1.00	0.00	0.58
Mean	1.03	3.49	1.08	0.96	1.24	0.26	1.32	1.58	3.58
Maximum	2.56	13.53	5.83	2.95	4.20	0.66	2.63	24.75	43.16

36 fractures were measured which strike in a NNE/SSW direction and dip steeply to the east, matching the NNE/SSW trend of the 1016 fracture orientations measured from the orthomosaic map (Fig. 7A). The observed fractures cross-cut the carbonate pipes, suggesting that the fractures post-date the pipes. From geological field data at Beloslav Quarry, the carbonate pipes display sub-vertical carbonate veining within open fractures (Fig. 7B and C). The veins are linear in shape, displaying no degree of sinuosity and no evidence of veins branching. The veins are commonly secondarily infilled with carbonate into previously open fractures. The veins appear to display a predominant north/south orientation. Within a (lower) carbonate bed, S-shearing is observed (Fig. 7D). Overall, there appears to be no clear diagenetic link between the fractures that cross-cut the pipes and formation of the pipes within the Dikilitash Formation.

Scanning electron microscopy analyses

Light microscopy and SEM imaging show that the host sediment and pipes have identical composition, differing only by the amount of carbonate cementation (low-Mg calcite cement; Fig. 6). The host sediment and pipes are composed of quartz grains (92%), with minor plagioclase feldspar (8%) and opaque minerals (0.1%). The grains are well-sorted and subangular, ranging from 100 to 140 μm in diameter. The host sediment has a very high porosity of 44.3%, reducing to 6.7% in the pipe, with precipitated low-Mg calcite cement occupying greater than 85% of the total pore volume. Using the known calculated porosity and average pore diameter (100 μm) values, the permeability of the uncemented sediments (k_u) is estimated using the Kozeny-Carman equation:

$$k_u = \left(\frac{1}{180}\right)\left(\frac{n_o{}^3}{(1-n_o)^2}\right)d^2 \qquad (1)$$

where n_o is total porosity and d is average pore diameter. While for cemented samples, the permeability (k_c) is given by:

$$k_c = k_u \left(\frac{\varepsilon}{\varepsilon_0}\right)^3 \left(\frac{1-\varepsilon_0}{1-\varepsilon}\right)^2 \qquad (2)$$

where ϵ is the total porosity of cemented sediments (new porosity) and ϵ_0 is the total porosity of the uncemented sediments (initial porosity). With increased calcite precipitation inside the pipes the permeability reduces by three orders of magnitude to 1.9×10^{-14} m² (0.02 darcy) relative to the surrounding host sediment of 1.5×10^{-11} m² (15 darcy). This equation is based on the reduction of porosity relative to the

Fig. 4. Uncrewed aerial vehicle (UAV)-based photogrammetric results from Beloslav Quarry. (A) Scatterplot for pipes and their nearest neighbour direction against nearest neighbour distance and corresponding histograms showing the frequency of both per unit. (B) Point cloud image of one prominent cliff showing six tiers of pipes (coloured triangles) corresponding to the intervals between the seven carbonate cemented interbeds (I1 to I7). See (D) for location. (C) UAV-based ortho-rectified image of Beloslav Quarry (BQ) with manually picked pipes and fractures. Black boxes show the location of (D) and (E), red triangles show pipe location, turquoise circle shows the location of Fig. 5. (D) Pipes picked in the point cloud separated by their elevation. Yellow dot marks the viewing location of (B). (E) Close-up of the densely-spaced pipes in the southern part of the outcrop.
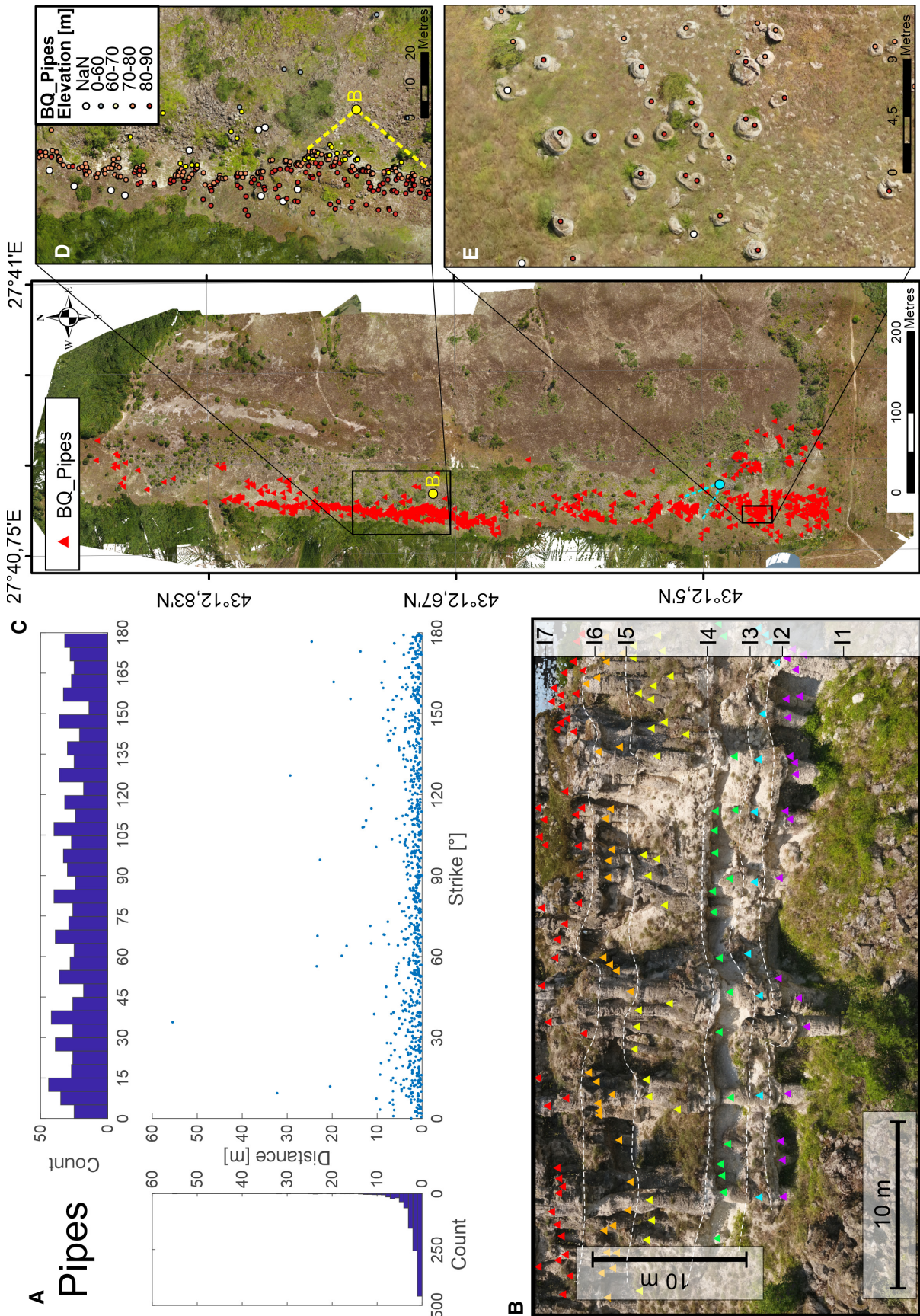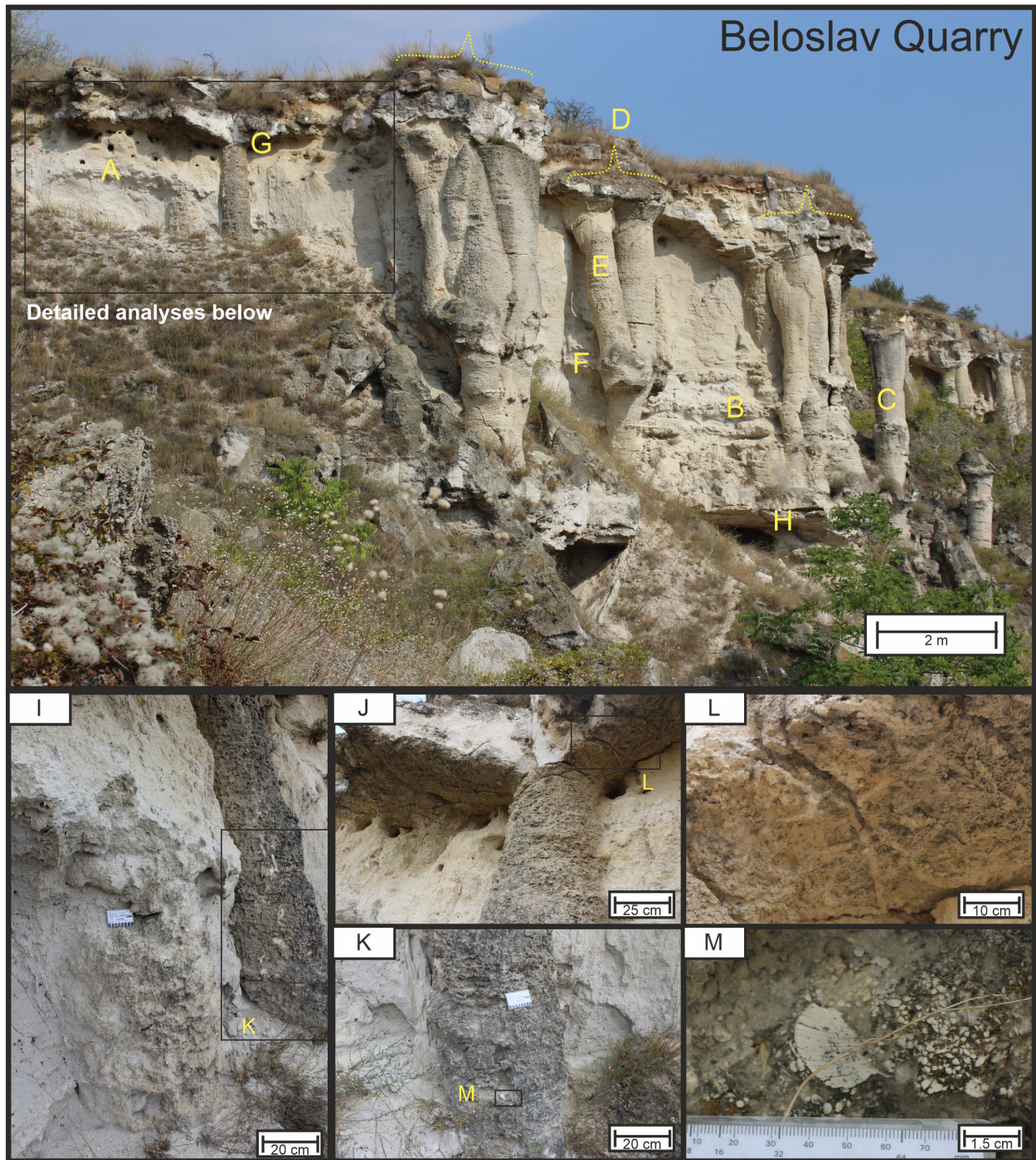
Fig. 5. Vantage point looking NNW within the Beloslav Quarry, providing an understanding of carbonate pipe geometry, and the relationship of the pipes with the surrounding sandy host rock, and the upper and lower carbonate horizontal interbeds. The letters (A) to (H) correspond to the main field observations described above. Detailed analyses indicated by black box. (I) Two carbonate pipes observed, one less weathered (in the foreground) and one more weathered (the dark grey coloured pipe). (J) The interface between the top of the carbonate pipe and the upper carbonate bed. The carbonate pipe emanates into the upper carbonate bed, despite the false appearance of a sharp contact due to a sub-horizontal fracture and white staining of the upper carbonate bed. (K) Another view of the carbonate pipe, appearing to have intruded vertically upward through the poorly consolidated sand host rock. (L) Horizontal branching burrow network at the base of the upper carbonate bed. (M) An abundance of shells and shell fragments 0.5 to 25 mm in size within the carbonate pipe, highlighting the similarity in composition between the pipe and the surrounding sandstone host rock.
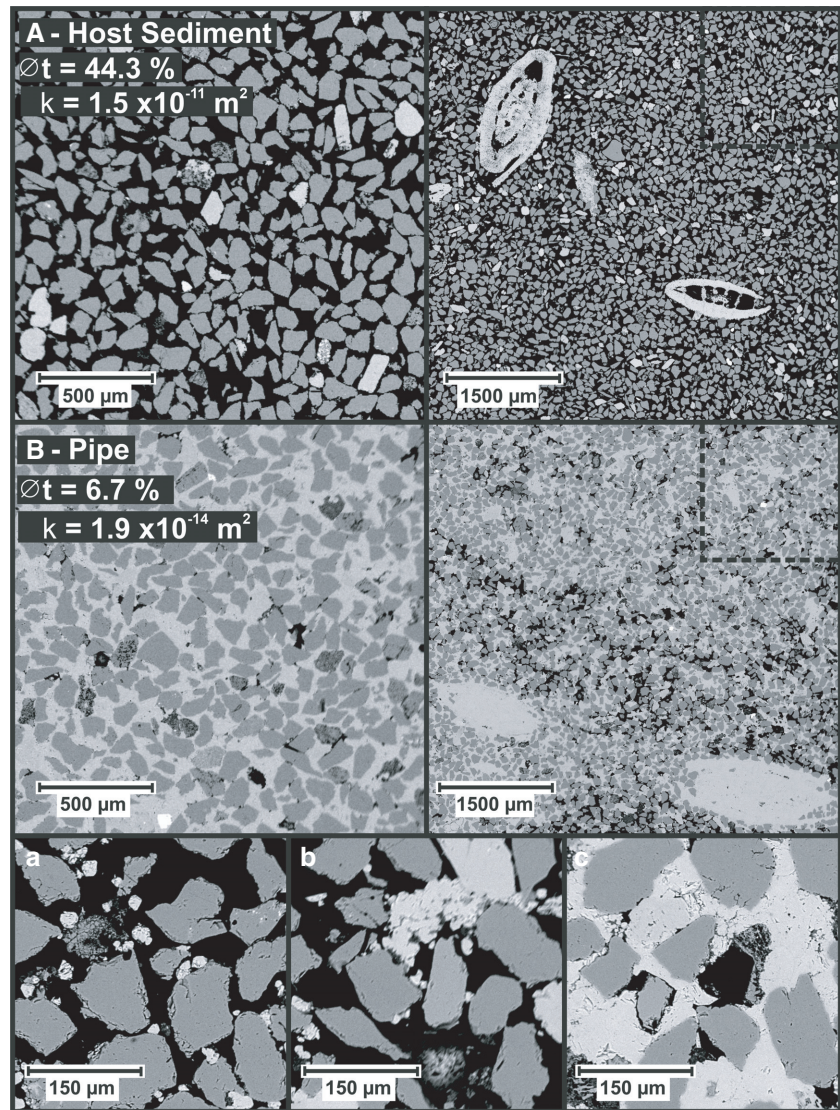
Fig. 6. Scanning electron microscopy (SEM) images displaying the textural similarity of the uncemented host sediment and the carbonate cemented pipes at Beloslav Quarry. (A) Well-sorted, poorly consolidated quartz sediment (100 to 140 µm grain size) with high porosity ($\varnothing t$) and estimated permeability (k) of 44.3% and 1.5×10^{-11} m^2 (15 darcy), respectively. Nummulite bioclasts are present in both samples. (B) Carbonate cement precipitation, occupying greater than 85% of the total pore volume, reducing permeability by three orders of magnitude (0.02 darcy). ('a' to 'c') shows the progressive cementation process of granular calcite within the intergranular pores.

uncemented sample, which is commonly used to estimate the effect of cementation on permeability (Phillips, 1991; Lichtner, 1996). The precipitation of calcite cement occurs progressively (Fig. 6A to C). Pre-existing grain surfaces commonly act as a substrate for the aggregation of calcite cement grains, although mineral precipitation independent of grain surfaces is also observed (Fig. 6A to C).

DISCUSSION

Distribution of pipes

Pipe distribution and spacing can provide an insight into the possible relationship between tectonic stress and pipe formation. Orthomosaic image analysis reveals comparable pipe diameters and spacings at Pobiti Kamani (3.58 ± 3.38 m) and Beloslav Quarry (2.24 ± 3.38 m), indicating that the controlling mechanisms for pipe formation are the same for both study areas. In both areas, the pipes are located along the north–south trending transtensional faults, within the Dikilitash Formation sediments. The pipes are situated on the eastern side hanging wall of the transtensional faults, that indicates a regional tectonic control on pipe location and genesis (Fig. 3). When observed on a localized scale, individual groups of pipes in both study areas are highly clustered (z-scores below −13). However, the orthomosaic maps and DEM reveal no apparent preferential orientation of the pipe
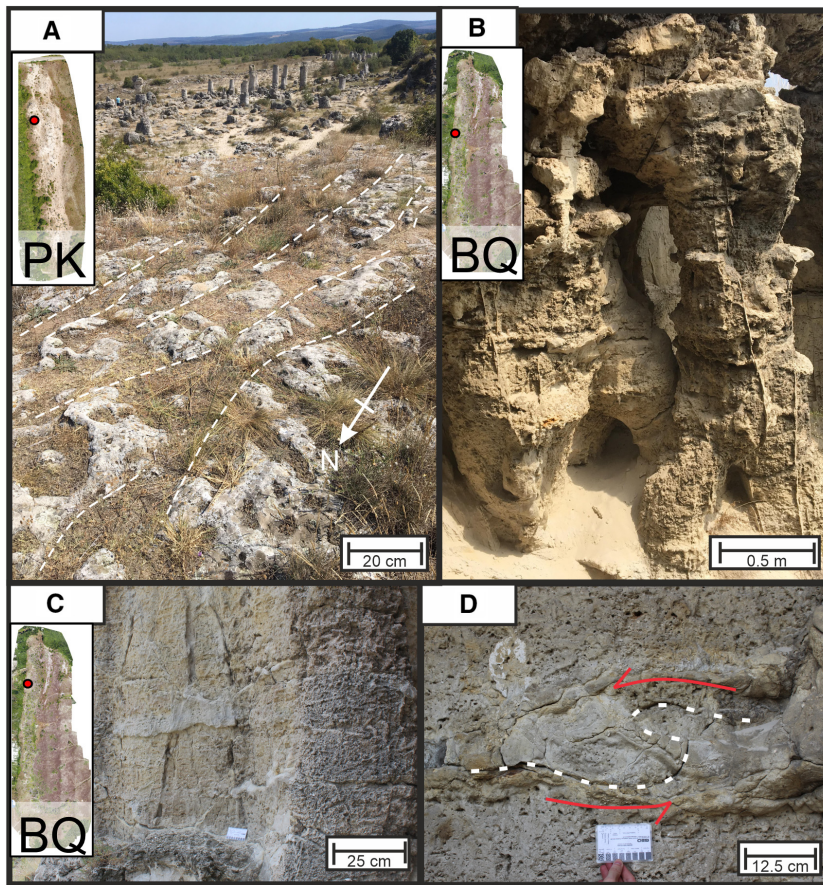
Fig. 7. (A) North/north-east trending fracture network on a carbonate interbed surface, at higher elevation than the carbonate pipes observed to the East. PK = Pobiti Kamani. Red dot in mini map indicates location of picture within the outcrop. (B) Metre-scale carbonate pipes displaying secondary sub-vertical carbonate veining within fractures. The veins are orientated NNE/SSW. BQ = Beloslav Quarry. Red dot in mini map indicates location of picture within the outcrop. (C) Fractures and carbonate veins observed, cross-cutting both the carbonate pipes and surrounding host rock, with no clear orientation trend. Red dot in mini map indicates location of picture within the outcrop. (D) S-shaped shear fabric within a carbonate horizon, indicating the presence of active north–south shear stress during the formation of this interval. (C) and (D) were taken at the same location.

clusters (nearest neighbour; Fig. 3). The findings oppose a localized structural control of pipe formation along pre-existing faults or fractures within the Dikilitash Formation, as suggested by De Boever *et al.* (2009b). Regionally developed fractures with an orientation of NNE–SSW are observed across the study areas (Fig. 3). The fractures cross-cut the pipes, and therefore post-date the pipes. Therefore, regional-scale tectonic deformation is interpreted as the controlling factor for the presence of pipes proximal to transtensional faults; however the pipes are unlikely to have formed along pre-existing planes of weakness within the Dikilitash Formation.

Pipe formation

Subaerial outcrop exposures of pipes provide an improved understanding of the conditions at the time of pipe formation. The host sediment of the Dikilitash Formation was deposited in a mid to outer ramp environment, evidenced by the lack of sediment bedding laminations, as well as the

presence and clustering of nummulite fossils. This type of depositional environment lays above the storm-wave base and is prone to the frequent reworking of sediments (Sinclair *et al.,* 1998). Therefore, the large height and the well-preserved status of the pipes (Fig. 5) argue against formation within the water column, because bottom currents in the mid to outer ramp environment would likely have resulted in erosion and low preservation potential. The sub-surface formation of the pipes is further supported by SEM imaging, showing that the pipes and host sediment have an identical grain composition and texture. The only difference between the pipes and surrounding sediment is the presence of low-Mg calcite that is observed to infill above 80% of the sediment pores, and that causes reductions in porosity and permeability by up to 40% and three orders of magnitude, respectively. Therefore, the analysis demonstrates that pipe-forming methane-derived authigenic carbonates (MDAC) likely precipitated within the unconsolidated sand of the Dikilitash Formation below the seafloor.

Previous work by De Boever *et al.* (2009a) further showed that the MDACs precipitated due to the microbially mediated anaerobic oxidization of methane (AOM).

Calcite cemented interbeds also observed in the study area reveal further information about the active history of the methane seep system. The presence of burrow (trace) fossils on the base of the interbeds provides key evidence to interpret that the horizons formed on the seabed, and hence represent the palaeo-seafloor. Additional field observations at Beloslav Quarry showed that the upper sections of pipes thicken and emanate into the overlying calcite cemented interbeds, showing a direct relationship between pipes and the interbeds (Fig. 5). Orthomosaic image mapping identified at least seven calcite cemented bedding-parallel interbeds separating the vertically stacked tiers of pipes (Figs 4 and 5). If each of these interbeds represents a palaeo-seafloor, it can be deduced that there were at least seven phases of methane emission from the methane seep system, and hence at least seven phases of pipe formation during the Early Eocene.

The assessment of pipe morphology and the physical properties of the host sediment may permit a further understanding of the nature of fluid flow that led to pipe formation. The high permeability (1.5×10^{-11} m^2) unconsolidated sand of the Dikilitash Formation should permit the advective flow of fluids. DEM and orthomosaic image mapping reveal that the pipes have a cylindrical (tube-like) geometry, displaying a large height to diameter ratio and low eccentricity. Further, the pipes also have a sub-vertical orientation, and are oriented perpendicular to bedding. The pipe morphology observations, correlated with the physical property measurements calculated from the SEM image analysis, further support advective flow, whereby mechanical dispersion is minimal. The SEM image analysis reveals that the sediment matrix has not been displaced by the fluids, which supports the interpretation of capillary-dominant flow, rather than fracture-dominant flow (Fauria & Rempel, 2011). Further, it is suggested that the pipes formed due to the focused, buoyancy-driven ascent of fluids (De Boever *et al.,* 2006a, 2009a). The sub-vertical ascent of fluids may also have been overpressure driven. However, high overpressures that would result in high flow velocities and turbulent flow are not supported by any observations, i.e. erosive fluidization (sediment remobilization; Lowe, 1975). The propagation of pressure waves or viscous flow of rising gas bubbles into the Dikilitash Formation may explain the formation of tube-shaped zones of vertical fluid flow (Boudreau *et al.,* 2005; Räss *et al.,* 2018).

Field observations show that the pipes have an outer layer of carbonates with a moderately diffuse boundary to unconsolidated sand in the interior (Fig. 5). Further quantified using the orthomosaic map, the pipes display predominantly unlithified cores (78%) and, less commonly, lithified inner cores (22%). Supported by the field observations, it is interpreted that carbonate precipitated on the outside of bubble streams at the interface of ascending fluids to ambient brackish or seawater, and likely resulted in a self-sustaining, positive feedback of focused fluid flow towards pipe centres (Clari *et al.,* 2004). Where methane flux rates were higher, the focused flow of methane likely prevented carbonate precipitation in the pipe centres (Luff & Wallmann, 2003). The observed large fraction of unlithified cores (78%), as well as the common field observation of bifurcation and merging of pipes, could be further used to interpret that fluid supply to the methane seep system from below was likely diverted rapidly to other migration pathways, that may include other pipes or the regional transtensional fault, which would be in accordance with the findings by De Boever *et al.* (2011b). Supported by the evidence of pipe clustering, it is interpreted that fluid flow was mainly focused along the Palaeogene transtensional faults and surrounding fractures beneath the Dikilitash Formation (for example, within the Beloslav Formation; Sinclair *et al.,* 1998, Fig. 1), that provided a source for the methane that entered the Dikilitash Formation at discrete zones.

The pipe formation processes interpreted in the study areas in Varna, Bulgaria, can be directly observed at modern, active seep systems. For example, focused fluid flow in marine sand formations is also documented from the 'bubbling reefs' in the Kattegat, offshore Denmark (Jørgensen, 1992). These pipes show ongoing discharge of methane and have formed below the seafloor. Constant erosion because of post-glacial isostatic uplift has exposed these features in 10 to 12 m water depth. The bubbling reef pipes can only be distinguished from their host sand by the amount of cementation. Some of the pipes are almost 4 m tall and 1.5 m in diameter (Jensen *et al.,* 1992). Carbon-isotope studies of the pipes identified a probable link between the bubbling gas ($\delta^{13}C_{CH4}$: −63 to
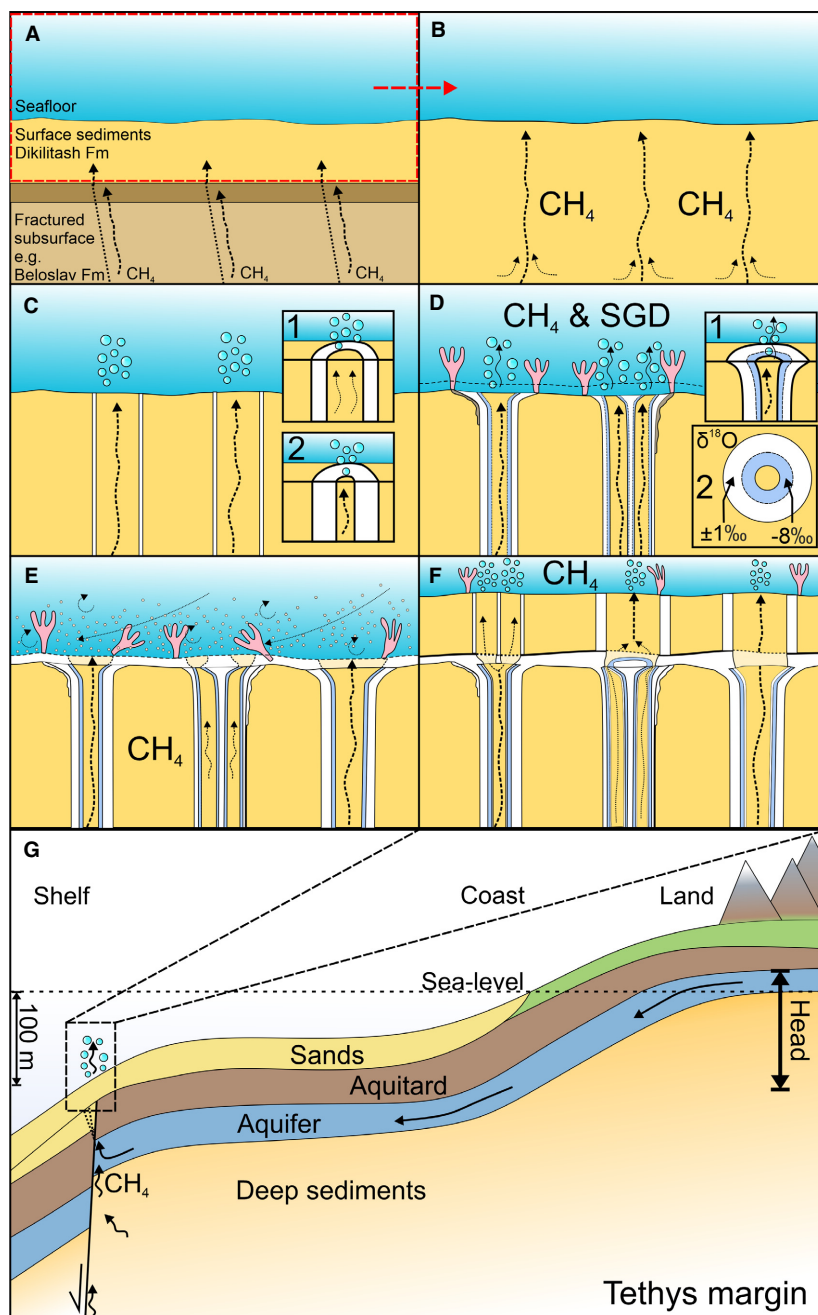
Fig. 8. Conceptual model showing the carbonate pipe formation through time – (B) to (F) modified after Clari *et al.,* 2004). (A) Methane ascends from below possibly along pre-existing planes of weakness in the subsurface due to transtensional tectonism in the Palaeogene. (B) Buoyancy driven focused upward migration of methane (CH₄) through poorly consolidated sandstone of the Dikilitash Formation. (C) Carbonate precipitation on the margins of methane gas seeps, forming the outer walls of the carbonate pipe. Progressive precipitation of carbonate towards the centre of the pipe through time ('1' to '2'). (D) Continued carbonate precipitation, widening at the seabed interface. Cold-seep benthic communities, such as tubeworms, form at the seabed around the methane release site. Benthic organisms may form vertical burrows or roots to allow uptake of hydrogen sulphide from the seep sediments. Episodic submarine groundwater discharge (SGD) leads to depleted oxygen isotope ratios in precipitated carbonates ('1' to '2'). (E) Bottom water currents provide additional sediment into the system, within an outer-ramp depositional setting. An outer carbonate crust forms at the seabed, interpreted to form from continued methane flux and precipitation of carbonate. (F) The process of pipe formation in the near subsurface repeats, methane continues to flow through preferential pathways created by older pipe structures. (G) Schematic model of coupled methane release and episodic submarine groundwater discharge at the shelf of the Tethys margin.

−75‰), the carbonates (δ¹³C: −26 to −63‰) and the methanotrophic bacteria ($\delta^{13}C_{OM}$: −43.4‰; Judd & Hovland, 2007). It can be suggested that focused fluid flow in sand and sandstone formations is not an exceptional case but also likely in other marine settings at the transition between tectonically faulted low permeable formations and overlying and higher-permeable formations (shale–sand interface). The focusing of fluids and subsequent formation of vertical conduits in high permeability formations largely depends on the focused advection of methane-rich fluid from below, for example, through pre-existing faults and fractures (Fig. 8A), the flux rate and progressive inward growth of carbonates (Fig. 8B to D).

Geological flow model

There are two alternating carbon and oxygen isotope signature groups (group 1: $\delta^{13}C$ *ca* −45 to −35‰ V-PDB and $\delta^{18}O$ ±1‰ V-PDB; group 2: $\delta^{13}C$ <−25‰ V-PDB and $\delta^{18}O$ <−6.5‰ V-PDB; De Boever *et al.,* 2009a), which appear in concentric bands around the centre of the pipes. Depleted $\delta^{18}O$ isotope ratios (<−6.5‰ V-PDB) can indicate carbonate precipitation in freshened, meteoric waters while more enriched values that plot closer to 0‰ V-PDB indicate the formation in brackish or seawater (Hays & Grossman, 1991). However, the process of late diagenetic secondary isotope re-equilibration at higher temperatures, which usually decreases the original $^{18}O/^{16}O$ ratio of the carbonates, has to be considered during burial of carbonate deposits (e.g. Fischer *et al.,* 2006). The observed alternating isotope signature groups can only be partly explained by percolating meteoric waters within the Dikilitash Formation (host sand) post-dating pipe formation (De Boever *et al.,* 2009a), as this would have only affected the outside of the pipes, assuming progressive precipitation of carbonate towards the centre of the pipe (Fig. 8) or resulted in a homogenization of isotopic signature groups. At the same time, the ascent of fluids with elevated temperatures would explain the different groups, but, in accordance with De Boever *et al.* (2006a), it is considered unlikely that fluids of different temperature ranges (hot/cold) share the same fluid migration system. In addition, this would have resulted in homogenization of carbon and oxygen isotope ratio groups, which is not observed. In contrast to previous interpretations, it can be suggested that the two signature groups were captured during

precipitation and are likely the cause of alternating fluid source characteristics. The alternating concentric rings of carbon and oxygen isotope signatures (De Boever *et al.,* 2006a) thus indicate episodic fresh/brackish water advection that fed the pipe structures from below.

The alternating carbonate isotope ratios in the pipes indicate that freshwater was episodically involved in the precipitation of carbonates (Fig. 8). Considering the presence and activity of the transtensional faults below the Dikilitash Formation, the freshwater was likely sourced from an aquifer below the Dikilitash Formation (for example, the Beloslav Formation or deeper; Sinclair *et al.,* 1998), which advected fluids from onshore resulting in episodic submarine groundwater discharge offshore. A similar coupled groundwater–methane discharge system is currently active along the eastern Bulgarian coastal areas documented by ongoing venting of methane (Dimitrov, 2002) and elevated radon isotope ratios (Moore & Falkner, 1999). In order to create topography-driven groundwater flow far out into the shelf (Hughes *et al.,* 2009; Morrissey *et al.,* 2010; Post *et al.,* 2013), for example, analogous to the New Jersey margin (Gustafson *et al.,* 2019), tectonic compression in the onshore realm during the Palaeogene (Sinclair *et al.,* 1998) likely provided the necessary hydraulic head (Fig. 8). This topography-driven groundwater flow likely forced episodic submarine groundwater discharge in addition to the methane emissions resulting in the two alternating characteristic isotope groups found in the carbonate pipes (Fig. 8).

CONCLUSIONS

The low-Mg calcite-cemented pipes of the Pobiti Kamani and Beloslav Quarry formed below the seafloor within unconsolidated sand of the Dikilitash Formation due to anaerobic microbial oxidation of methane fed by methane-rich fluids that were advected from deeper sources. Because the pipes occur within the vicinity of major fault deformation of the unit underlying the Dikilitash Formation, this has probably focused the fluid flow at certain points. Efficient microbial turnover of methane to carbonate within the shallow marine sediment has maintained the focused flow paths. This explains the large diameters and size of the pipes despite their dense spacing. The calcite cemented interbeds likely represent palaeo-seafloors. Thus,

there have been at least seven phases of increased carbonate precipitation during phases of sea-level changes in the past.

Regional tectonic deformation likely played a key role in controlling the location of the pipe clusters on a regional scale. The pipe clusters tend to form towards the eastern side of major transtensional faults in the sand of the Dikilitash Formation. However, on a local scale, tectonic deformation does not govern the distribution of the pipes within the unconsolidated sand.

The calcite cementation of the conduits show two distinct groups of carbon and oxygen isotopes that appear in concentric bands around the centre of the pipes. These groups likely represent different phases of episodic fluid release with different characters. The isotope systematics suggest that the first group of methane-derived authigenic carbonates (MDAC) formed from biogenic methane and ambient seawater dissolved inorganic carbon (DIC). The second group of MDAC formed during the episodic release of groundwater mixed with methane-rich fluids.

Analogous with the New Jersey margin (Gustafson *et al.,* 2019), groundwater was likely advected to the mid to outer ramp shelf setting through an aquifer driven by topographic changes in the onshore realm. Sufficient groundwater heads likely existed because of active deformation and uplift during the Eocene. Focused fluid flow in sand and sandstone formations is not an exception but it is also likely present in current marine settings at the transition between low and high-permeable formations (for example, shale–sand interface) where methane seepage is combined with submarine groundwater discharge.

ACKNOWLEDGEMENTS

DATA AVAILABILITY STATEMENT

The data that support the findings of this study are available from the corresponding author upon reasonable request.

REFERENCES

Andresen, K.J. (2012) Fluid flow features in hydrocarbon plumbing systems: what do they tell us about the basin evolution? *Mar. Geol.*, **332**, 89–108.

Angeletti, L., Canese, S., Franchi, F., Montagna, P., Reitner, J., Walliser, E.O. and **Taviani, M.** (2015) The "chimney forest" of the deep Montenegrin margin, south-eastern Adriatic Sea. *Mar. Petrol. Geol.*, **66**, 542–554.

Bemis, S.P., Micklethwaite, S., Turner, D., James, M.R., Akciz, S., Thiele, S.T. and **Bangash, H.A.** (2014) Ground-based and UAV-based photogrammetry: a multi-scale, high-resolution mapping tool for structural geology and paleoseismology. *J. Struct. Geol.*, **69**, 163–178.

Bergerat, F., Martin, P. and **Dimov, D.** (1998) The Moesian Platform as a key for understanding the geodynamical evolution of the Carpatho-Balkan alpine system. *Mémoires du Muséum national d'histoire naturelle*, **177**, 129–150.

Berndt, C. (2005) Focused fluid flow in passive continental margins. *Philos. Trans. R. Soc. Lond. A Math. Phys. Eng. Sci.*, **363**, 2855–2871.

Bisdom, K., Nick, H.M. and **Bertotti, G.** (2017) An integrated workflow for stress and flow modelling using outcrop-derived discrete fracture networks. *Comput. Geosci.*, **103**, 21–35.

Böttner, C., Berndt, C., Reinardy, B.T., Geersen, J., Karstens, J., Bull, J.M., Callow, B.J., Lichtschlag, A., Schmidt, M., Elger, J., Schramm, B. and **Haeckel, M.** (2019) Pockmarks in the Witch Ground Basin, Central North Sea. *Geochem. Geophys. Geosyst.*, **20**, 1698–1719.

Botz, R.W., Georgiev, V., Stoffers, P., Khrischev, K. and **Kostadinov, V.** (1993) Stable isotope study of carbonate-cemented rocks from the Pobitite Kamani area, north-eastern Bulgaria. *Geol. Rundsch.*, **82**, 663–666.

Boudreau, B.P., Algar, C., Johnson, B.D., Croudace, I., Reed, A., Furukawa, Y., Dorgan, K.M., Jumars, P.A., Grader, A.S. and Gardiner, B.S. (2005) Bubble growth and rise in soft sediments. *Geology*, **33**(6), 517–520.

Callow, B., Falcon-Suarez, I., Marin-Moreno, H., Bull, J.M. and Ahmed, S. (2020) Optimal X-ray micro-CT image based methods for porosity and permeability quantification in heterogeneous sandstones. *Geophys. J. Int.*, **223**, 1210–1229.

Capozzi, R., Negri, A., Reitner, J. and Taviani, M. (2015) Carbonate conduits linked to hydrocarbon-enriched Fluid Escape. *Mar. Petrol. Geol.*, **66**, 497–500.

Cartwright, J. (2007) The impact of 3D seismic data on the understanding of compaction, fluid flow and diagenesis in sedimentary basins. *J. Geol. Soc.*, **164**, 881–893.

Clari, P., Cavagna, S., Martire, L. and Hunziker, J. (2004) A Miocene Mud Volcano and its plumbing system: a chaotic complex revisited (Monferrato, NW Italy). *J. Sed. Res.*, **74**, 662–676.

De Boever, E., Birgel, D., Thiel, V., Muchez, P., Peckmann, J., Dimitrov, L. and Swennen, R. (2009a) The formation of giant tubular concretions triggered by anaerobic oxidation of methane as revealed by archaeal molecular fossils (Lower Eocene, Varna, Bulgaria). *Palaeogeogr. Palaeoclimatol. Palaeoecol.*, **280**, 23–36.

De Boever, E., Birgel, D., Muchez, P., Peckmann, J., Dimitrov, L. and Swennen, R. (2011a) Fabric and formation of grapestone concretions within an unusual ancient methane seep system (Eocene, Bulgaria). *Terra Nova*, **23**, 56–61.

De Boever, E., Huysmans, M., Muchez, P., Dimitrov, L. and Swennen, R. (2009b) Controlling factors on the morphology and spatial distribution of methane-related tubular concretions—case study of an Early Eocene seep system. *Mar. Petrol. Geol.*, **26**, 1580–1591.

De Boever, E., Muchez, P., Swennen, R. and Dimitrov, L. (2011b) Evolution of deformation and fault-related fluid flow within an ancient methane seep system (Eocene, Varna, Bulgaria). *Geofluids*, **11**, 166–183.

De Boever, E., Swennen, R. and Dimitrov, L. (2006a) Lower Eocene carbonate cemented chimneys (Varna, NE Bulgaria): formation mechanisms and the (a) biological mediation of chimney growth? *Sed. Geol.*, **185**, 159–173.

De Boever, E., Swennen, R. and Dimitrov, L. (2006b) Lower Eocene carbonate-cemented "chimney" structures (Varna, Bulgaria)—control of seepage rates on their formation and stable isotopic signature. *J. Geochem. Explor.*, **89**, 78–82.

Dimitrov, L. (2002) Contribution to atmospheric methane by natural seepages on the Bulgarian continental shelf. *Cont. Shelf Res.*, **22**, 2429–2442.

Fauria, K.E. and Rempel, A.W. (2011) Gas invasion into water-saturated, unconsolidated porous media: Implications for gas hydrate reservoirs. *Earth Planet Sci. Lett.*, **312**, 188–193.

Fischer, M., Botz, R., Schmidt, M., Rockenbauch, K., Garbe-Schönberg, D., Glodny, J., Gerling, P. and Littke, R. (2006) Origins of CO_2 in permian carbonate reservoir rocks (Zechstein, Ca2) of the NW-German Basin (Lower Saxony). *Chem. Geol.*, **227**, 184–213.

Georgiev, G., Dabovski, C. and Stanisheva-Vassileva, G. (2001) East Srednogorie-Balkan rift zone. *Mém. Mus. Natl d'histoire Nat.*, **186**, 259–293.

Gustafson, C., Key, K. and Evans, R.L. (2019) Aquifer systems extending far offshore on the U.S. Atlantic margin. *Sci. Rep.*, **9**, 1–10.

Hays, P.D. and Grossman, E.L. (1991) Oxygen isotopes in meteoric calcite cements as indicators of continental paleoclimate. *Geology*, **19**, 441–444.

Hughes, J.D., Vacher, H.L. and Sanford, W.E. (2009) Temporal response of hydraulic head, temperature, and chloride concentrations to sea-level changes, Floridan aquifer system, USA. *Hydrogeol. J.*, **17**, 793–815.

Huuse, M., Jackson, C.A.L., Van Rensbergen, P., Davies, R.J., Flemings, P.B. and Dixon, R.J. (2010) Subsurface sediment remobilization and fluid flow in sedimentary basins: an overview. *Basin Res.*, **22**, 342–360.

Jensen, P., Aagaard, I., Burke Jr., R.A., Dando, P.R., Jorgensen, N.O., Kuijpers, A., Laier, T., O'Hara, S.C.M. and Schmaljohann, R. (1992) 'Bubbling reefs' in the Kattegat: submarine landscapes of carbonate-cemented rocks support a diverse ecosystem at methane seeps. *Mar. Ecol. Prog. Ser.*, **83**, 102–112.

Jørgensen, N.O. (1992) Methane-derived carbonate cementation of marine sediments from the Kattegat, Denmark: geochemical and geological evidence. *Mar. Geol.*, **103**, 1–13.

Judd, A. and Hovland, M. (2007) *Seabed Fluid Flow: The Impact on Geology, Biology and the Marine Environment*. Cambridge: Cambridge University Press.

Karstens, J. and Berndt, C. (2015) Seismic chimneys in the Southern Viking Graben-Implications for palaeo fluid migration and overpressure evolution. *Earth Planet Sci. Lett.*, **412**, 88–100.

Ketcham, R.A. and Carlson, W.D. (2001) Acquisition, optimization and interpretation of X-ray computed tomographic imagery: applications to the geosciences. *Comput. Geosci.*, **27**, 381–400.

Lichtner, P.C. (1996) Continuum formulation of multicomponent-multiphase reactive transport. *Rev. Mineral.*, **34**, 1–82.

Lowe, D.R. (1975) Water escape structures in coarse-grained sediments. *Sedimentology*, **22**, 157–204.

Luff, R. and Wallmann, K. (2003) Fluid flow, methane fluxes, carbonate precipitation and biogeochemical turnover in gas hydrate-bearing sediments at Hydrate Ridge, Cascadia Margin: numerical modeling and mass balances. *Geochim. Cosmochim. Acta*, **67**, 3403–3421.

Moore, W.S. and Falkner, K.K. (1999) Cycling of radium and barium in the Black Sea. *J. Environ. Radioact.*, **43**, 247–254.

Morrissey, S.K., Clark, J.F., Bennett, M., Richardson, E. and Stute, M. (2010) Groundwater reorganization in the Floridan aquifer following Holocene sea-level rise. *Nat. Geosci.*, **3**, 683–687.

Nelson, C.S., Nyman, S.L., Campbell, K.A. and Rowland, J.R. (2017) Influence of faulting on the distribution and development of cold seep-related dolomitic conduit concretions at East Cape, New Zealand. *N. Z. J. Geol. Geophys.*, **60**, 478–496.

Phillips, O.M. (1991) *Flow and Reactions in Permeable Rocks*. Cambridge: Cambridge University Press.

Planke, S. and Berndt, C. (2007) *U.S. Patent No. 7,221,620*. U.S. Patent and Trademark Office, Washington, DC.

Post, V.E., Groen, J., Kooi, H., Person, M., Ge, S. and Edmunds, W.M. (2013) Offshore fresh groundwater reserves as a global phenomenon. *Nature*, **504**, 71–78.

Räss, L., Simon, N.S. and Podladchikov, Y.Y. (2018) Spontaneous formation of fluid escape pipes from subsurface reservoirs. *Sci. Rep.*, **8**, 11116.

Sinclair, H.D., Juranov, S.G., Georgiev, G., Byrne, P. and Mountney, N.P. (1998) The Balkan thrust wedge and foreland basin of eastern Bulgaria: structural and

stratigraphic development. *Mem. Am. Assoc. Petrol. Geol.,* **68**, 91–114.

Whitaker, S. (1986) Flow in porous media I: a theoretical derivation of Darcy's law. *Transp. Porous Media*, **1**, 3–25.

White, J.E. (1975) Computed seismic speeds and attenuation in rocks with partial gas saturation. *Geophysics*, **40**, 224–232.

Supporting Information

Additional information may be found in the online version of this article:

Supinfo S1. Beloslav Quarry – 3D topographic model.

Supinfo S2. Pobiti Kamani – 3D topographic model.